Journal of Biotechnology and Natural Science
Vol. 6, No. 1, June 2026, pp. 45-54
ISSN 2808-2508

Integrative In Silico Analysis of Klotho KL-VS Variants rs9527025 and rs9536314: Structural, Expression, and Network Insights

Bramadi Arya[1]*, Rita Maliza[2]

[1]Department of Medical Laboratory Technology, Universitas Syedza Saintika, Padang
[2]Department of Biology, Faculty of Mathematics and Natural Sciences, Universitas Andalas, Padang
[1]arya@syedzasaintika.ac.id*; [2]ritamaliza@sci.unand.ac.id
*corresponding author

ARTICLE INFO

Article history
Received: April 20st 2026
Revised: June 1st 2026
Accepted: June 29th 2026

Keywords
In silico analysis
Klotho
KL-VS
Protein structure
SNP

ABSTRACT

The Klotho (*KL*) gene encodes α-Klotho, a transmembrane protein that functions as an obligate co-receptor for fibroblast growth factor 23 (FGF23), thereby regulating phosphate homeostasis, vitamin D metabolism, and aging-related signaling. The KL-VS haplotype contains two coding variants, rs9536314 (Phe352Val) and rs9527025 (Cys370Ser), with previously reported opposing effects on Klotho secretion: F352V impairs secretion through intracellular retention, whereas C370S enhances extracellular Klotho levels. However, the structural basis underlying these contrasting phenotypes remains incompletely defined, and non-KL-VS substitutions at the multiallelic rs9527025 site have not been systematically evaluated. This study performed an integrative in silico characterization of rs9527025 and rs9536314 within the KL1 domain of α-Klotho using multi-algorithm functional prediction, thermodynamic perturbation analysis, tissue-specific expression profiling, and gene interaction network analysis. Substitutions at Phe352, particularly F352V, showed the most consistent predicted functional damage and thermodynamic perturbation, with ΔΔG values reaching −3.02 kcal/mol, supporting a structural model in which disruption of the KL1 hydrophobic core contributes to the secretion-impairing phenotype. In contrast, C370S showed minimal predicted perturbation, consistent with its reported secretion-enhancing effect, whereas C370Y and C370F produced lower-confidence and partly discordant predictions suggestive of localized effects. GTEx v10 analysis confirmed predominant *KL* expression in kidney cortex, while GeneMANIA network analysis showed dense connectivity between *KL*, FGF23, and FGFR1–FGFR4. As a computational study, these findings provide a hypothesis-generating structural framework anchored to previously reported KL-VS secretion phenotypes and support future experimental validation of Klotho folding, trafficking, and FGF23–FGFR co-receptor assembly.

How to Cite: Arya, B. & Maliza, R. (2026). Integrative In Silico Analysis of Klotho KL-VS Variants rs9527025 and rs9536314: Structural, Expression, and Network Insights. *Journal of Biotechnology and Natural Science*, 6(1):45-54.

1. Introduction

The Klotho (*KL*) gene encodes α-Klotho, a type-I transmembrane protein that serves as an obligate co-receptor for fibroblast growth factor 23 (FGF23) and is a central regulator of phosphate homeostasis, vitamin D metabolism, and aging-related pathways (Kuro-o et al., 1997; Xu & Sun, 2015). The gene was originally identified through a mouse model harboring a promoter mutation that produced a premature aging syndrome including atherosclerosis, osteoporosis, infertility, and shortened lifespan (Kuro-o et al., 1997). In humans, circulating α-Klotho levels decline progressively with age after the fourth decade and are associated with the progression of chronic kidney disease, vascular calcification,

and metabolic disorders (Hu et al., 2011). The soluble form of α-Klotho, generated by proteolytic shedding via ADAM10 and ADAM17, functions as a humoral factor with pleiotropic effects on oxidative stress, inflammation, and growth factor signaling (Dalton et al., 2017; Xu & Sun, 2015). Beyond mineral metabolism, α-Klotho has been implicated in oxidative stress regulation, inflammation, fibrosis, and Wnt/β-catenin signaling, suggesting that its biological functions extend beyond the renal phosphate–vitamin D axis (Doi et al., 2011; Tang et al., 2016; Kuro-o, 2019).

KL encodes a protein with two tandem glycosidase-homology domains, KL1 and KL2, through which it facilitates FGF23 binding to fibroblast growth factor receptors (FGFRs) and activates downstream MAPK/ERK signaling to regulate phosphate excretion and 1,25-dihydroxyvitamin D production (Xu & Sun, 2015; Kuro-o, 2019). The KL1 domain in particular contributes directly to the formation of the FGF23-FGFR-Klotho ternary signaling complex by increasing FGF23 binding affinity to FGFRs. Perturbations within this domain are therefore of direct functional significance to the phosphate-vitamin D endocrine axis.

A well-characterized functional haplotype of *KL*, termed KL-VS, encompasses six single nucleotide variants in complete linkage disequilibrium within exon 2, two of which produce amino acid substitutions: rs9536314 (Phe352Val, F352V) and rs9527025 (Cys370Ser, C370S) (Arking et al., 2002). Cell-based functional assays using transient transfection of V5-tagged secreted Klotho constructs in HeLa cells demonstrated that these two substitutions have opposing effects on extracellular Klotho levels. The F352V substitution markedly reduces secreted Klotho (greater than 6-fold decrease) with concurrent intracellular accumulation (approximately 1.56-fold increase), consistent with impaired secretion through intracellular retention or a trafficking defect. In contrast, C370S increases extracellular Klotho (approximately 2.9-fold). When both substitutions are combined as the KL-VS double mutant, an intermediate secretion phenotype is observed (approximately 1.6-fold increase), interpreted as partial intragenic complementation in cis (Arking et al., 2002). Importantly, the analogous F289V substitution in the closest human Klotho paralog with a known substrate (cBGL1) completely abolished enzymatic activity, further demonstrating the functional importance of Phe352 (Arking et al., 2002). Across the literature, the primary functional consequence of KL-VS variants is therefore an alteration in protein secretion and intracellular trafficking rather than a direct biophysical destabilization of the folded protein, and effects appear modest and context-dependent at the population level (Wu et al., 2020). Beyond mineral metabolism, carrying a single copy of the KL-VS haplotype (KL-VS heterozygosity) has been linked to aging- and cognition-related phenotypes, including reduced amyloid-dependent tau accumulation and memory impairment in Alzheimer's disease (Neitzel et al., 2021). This broader biological relevance strengthens the rationale for structurally interpreting the KL-VS coding substitutions F352V and C370S.

Three specific gaps motivate the present study. First, no prior computational study has explicitly framed F352V and C370S in terms of the contrasting secretion phenotypes established by Arking et al. (2002), nor proposed a structural rationale for why these two substitutions produce opposite trafficking outcomes. Second, the non-KL-VS substitutions at the multiallelic rs9527025 site (C370Y and C370F) have neither been experimentally characterized nor computationally evaluated. Third, no previous work has integrated multi-algorithm functional prediction, predicted thermodynamic perturbation, tissue-specific expression, and gene interaction network analysis into a single interpretive framework for these variants. Here, we address these gaps through an integrative in silico characterization of rs9527025 and rs9536314 within the KL1 domain of human α-Klotho. Multi-algorithm functional prediction and thermodynamic perturbation analysis were interpreted in relation to the experimentally reported secretion phenotypes of the KL-VS variants, particularly the secretion-impairing effect of F352V and the secretion-enhancing effect of C370S. Tissue-specific expression profiling and gene interaction network analysis were further integrated to place these structural predictions within the biological context of the renal FGF23–Klotho endocrine axis. This framework was designed to generate mechanistic hypotheses and prioritize Klotho variants for future experimental validation.

2. Methods

2.1. SNP Selection and Variant Annotation

Missense single nucleotide polymorphisms (nsSNPs) in the human *KL* gene were retrieved from the NCBI dbSNP database (https://www.ncbi.nlm.nih.gov/snp/) using the search term "Klotho (*KL*)," filtered for missense variants. The study focused on rs9527025 and rs9536314, the two coding amino acid changes of the KL-VS haplotype and the most functionally characterized natural variants of the KL gene (Arking et al., 2002). Given the multiallelic nature of rs9527025, all three possible amino acid outcomes at position 370 (C370Y, C370S, C370F) were included for analysis. Variant nomenclature followed Human Genome Variation Society (HGVS) guidelines using reference sequences NM_004795.4 (mRNA) and NP_004786.2 (protein).

2.2. Multi-Algorithm Functional Prediction

Functional impact was evaluated using five in silico tools selected to represent complementary and methodologically independent approaches, so that concordance across tools strengthens confidence while discordance reveals prediction uncertainty. PolyPhen-2 (Polymorphism Phenotyping v2) was selected because it integrates both sequence-based evolutionary conservation and structural features of the protein, providing a hybrid sequence-structure prediction; it classifies variants as benign (0.0 to 0.15), possibly damaging (0.15 to 0.85), or probably damaging (0.85 to 1.0). PROVEAN (Protein Variation Effect Analyzer) was selected as a purely alignment-based tool that evaluates whether a substitution shifts the biological function of the protein relative to homologous sequences, classifying variants as deleterious at scores of -2.5 or below; its independence from structural assumptions complements PolyPhen-2. PhD-SNP was selected because it applies profile-based machine learning trained on disease-variant databases, providing a pathogenicity classification that is not directly dependent on conservation scoring. SNPs&GO was selected because it incorporates functional Gene Ontology information alongside sequence context, offering a disease-association probability score that accounts for the biological role of the protein. PANTHER was selected to assess the evolutionary conservation score of the substituted residue specifically within the protein family context, providing an evolutionary pressure metric independent of disease databases. Using tools with distinct algorithmic foundations means that consistent predictions across multiple approaches reflect robust evidence, while inconsistencies across tools are themselves informative about the complexity of the variant's predicted impact. Variants consistently predicted as damaging across multiple independent tools were designated as potentially functionally disruptive variants. For operational consistency, the following interpretation thresholds were applied: PolyPhen-2 scores above 0.85 were classified as probably damaging; PROVEAN scores at or below -2.5 were classified as deleterious; PhD-SNP and SNPs&GO classifications of "disease" were recorded with their corresponding reliability/probability scores as returned by the default server settings. All analyses were performed using publicly available web servers accessed between January and March 2026, using default parameters unless explicitly stated otherwise.

2.3. Predicted Thermodynamic Perturbation Analysis

Predicted changes in protein thermodynamic stability (ΔΔG, kcal/mol) upon amino acid substitution were estimated using two methodologically distinct tools to enable cross-validation. I-Mutant v2.0 (Capriotti et al., 2005) was applied to the reference α-Klotho protein sequence (UniProt Q9UEF7) using default parameters. DynaMut2 (Rodrigues et al., 2021), accessed via https://biosig.lab.uq.edu.au/dynamut2/, was applied to the AlphaFold-predicted structure of human α-Klotho (model AF-Q9UEF7-F1, canonical isoform, 1012 residues) with chain A specified and default parameters; the local model confidence (pLDDT) exceeded 95 at both positions 352 and 370, indicating very high structural reliability at the residues of interest. I-Mutant v2.0 is a sequence/structure-based support vector machine trained on ProTherm, whereas DynaMut2 integrates normal-mode analysis of protein flexibility with graph-based signatures of the wild-type residue environment; the two tools therefore approach ΔΔG estimation from independent computational assumptions, so concordant predictions strengthen confidence while discordant predictions flag uncertainty. Positive ΔΔG values indicate predicted stabilization and negative values indicate predicted destabilization. Because DynaMut2 classifies any negative ΔΔG as destabilizing without a magnitude threshold, and given its reported RMSE of approximately 1.0–1.14 kcal/mol, predicted changes smaller than approximately 1 kcal/mol were interpreted as minimal perturbation within the tool's error margin, consistent with established conventions in the protein-stability prediction literature

(Tokuriki & Tawfik, 2009). These ΔΔG values were interpreted as computational estimates of relative thermodynamic perturbation and were used to support structural prioritization rather than to establish direct biophysical stability.

2.4. Tissue-Specific Expression Analysis

Tissue-specific expression of *KL* (ENSG00000133116.8) was analyzed using the Genotype-Tissue Expression (GTEx) Portal, Analysis Release V10 (https://www.gtexportal.org), covering RNA-seq data across 54 human tissues. Median TPM values were used to identify tissues with the highest expression and to contextualize the biological relevance of the studied variants in specific physiological compartments.

2.5. Gene Interaction Network

Functional gene interaction networks were constructed using GeneMANIA (https://genemania.org; web application version 3.6.0; database version 13 August 2021; accessed May 29, 2026). The query gene was *KL* with Homo sapiens as the organism, default settings, and all seven interaction categories enabled (physical interactions, co-expression, co-localization, predicted interactions, genetic interactions, shared pathway, and shared protein domains). Network weight composition, which the GeneMANIA documentation defines as the relevance of each data source for predicting the function of the query gene, was recorded directly from the GeneMANIA interface. In addition, the complete network was exported as a tab-delimited text file and the raw edge counts per category were extracted programmatically; both metrics are reported in Section 3.4.

3. Results and Discussion

3.1. Variant Annotation and Structural Context

HGVS annotation confirmed that rs9527025 and rs9536314 both generate missense variants within the KL1 domain of α-Klotho (NP_004786.2), as shown in **Table 1**. The variant rs9527025 is multiallelic at position c.1109 (NM_004795.4), producing p.Cys370Tyr (C370Y), p.Cys370Ser (C370S), and p.Cys370Phe (C370F). The variant rs9536314 occurs at position c.1054, producing p.Phe352Ile (F352I) and p.Phe352Val (F352V).

The experimental context is essential for interpreting the computational results. Among the five substitutions analyzed, C370S and F352V, the two coding changes of the KL-VS haplotype, have been functionally characterized in cell-based assays. F352V was reported to reduce secreted Klotho by more than six-fold with concurrent intracellular accumulation, whereas C370S increased extracellular Klotho by approximately 2.9-fold (Arking et al., 2002). Therefore, the computational analyses in this study were interpreted against these established secretion phenotypes. The remaining substitutions, C370Y, C370F, and F352I, are currently uncharacterized experimentally and were evaluated as computationally prioritized candidates for future functional assessment.

Structurally, Phe352 is located in the hydrophobic core of KL1 (Figure 1) and participates in aromatic packing interactions that stabilize the domain fold.

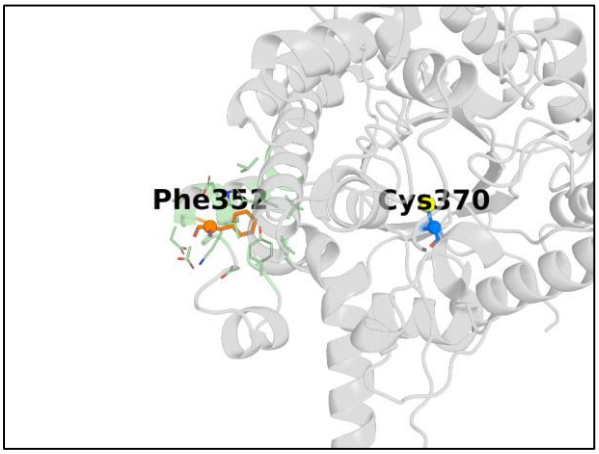

Figure 1. Structural localization of Phe352 and Cys370 in the KL1 domain of human α-Klotho. The AlphaFold-predicted model (UniProt Q9UEF7; local pLDDT > 95 at both positions) is shown as a grey

cartoon. Phe352 (orange sticks) is buried within the hydrophobic core, surrounded by packing partners within 5 Å (pale green sticks), consistent with its predicted role in maintaining the KL1 fold. Cys370 (blue sticks; sulfur atom in yellow) occupies a comparatively surface-proximal position, consistent with greater tolerance to substitution. The contrasting structural environments are concordant with the differential ΔΔG predictions reported in Table 2. Rendered with PyMOL v3.

Substitution by valine or isoleucine removes the aromatic ring, potentially disrupting pi-stacking and hydrophobic packing (Tokuriki & Tawfik, 2009). Cys370, in contrast, occupies a position that corresponds to serine in the mouse Klotho ortholog, suggesting that the site tolerates small polar substitutions (Arking et al., 2002). Substitution to tyrosine or phenylalanine would introduce bulky aromatic side chains that could introduce steric strain in the local structural context, while C370S is predicted to produce a more modest localized change (Betz, 1993). The KL1 domain also forms the interface that enhances FGF23 binding affinity to FGFRs (Xu & Sun, 2015; Kuro-o, 2019), making any perturbation within this domain functionally relevant to downstream signaling.

Table 1. HGVS annotation of missense variants rs9527025 and rs9536314 in the *KL* gene.

SNP ID	Nucleotide Change	Codon Change	Protein Change	Variant Type
rs9527025	c.1109G>A	TGC → TAC	p.Cys370Tyr (C370Y)	Missense
	c.1109G>C	TGC → TCC	p.Cys370Ser (C370S)	Missense
	c.1109G>T	TGC → TTC	p.Cys370Phe (C370F)	Missense
rs9536314	c.1054T>A	TTT → ATT	p.Phe352Ile (F352I)	Missense
	c.1054T>G	TTT → GTT	p.Phe352Val (F352V)	Missense

Note: KL-VS = substitution present in the naturally occurring KL-VS haplotype, functionally characterized in Arking et al. (2002). Nucleotide positions refer to NM_004795.4; protein positions refer to NP_004786.2

3.2. Multi-Algorithm Functional Prediction and Structural Perturbation

To strengthen the thermodynamic interpretation and to address the limitation of relying on a single predictor, ΔΔG changes were additionally estimated using DynaMut2, which is methodologically independent of I-Mutant v2.0 in that it combines normal-mode analysis with graph-based structural signatures of the wild-type residue environment rather than a sequence/structure-based support vector machine. The cross-tool pattern supports a structural distinction between the two loci. For the Phe352 substitutions, both predictors concordantly estimated the largest destabilization: F352V yielded ΔΔG values of −3.02 kcal/mol (I-Mutant v2.0) and −1.52 kcal/mol (DynaMut2), while F352I yielded −1.56 and −1.25 kcal/mol, respectively. The convergence of both tools on relatively large negative values, combined with the consistent “deleterious” and “probably damaging” classifications across the functional predictors, suggests that position 352 is under strong structural constraint and that F352V is predicted to be particularly susceptible to perturbation of the KL1 hydrophobic core (Figure 1). This interpretation is reinforced by the DynaMut2 interaction analysis, which shows Phe352 embedded within an extensive network of hydrophobic and aromatic contacts whose loss upon substitution by a smaller aliphatic residue could create a packing defect; however, this remains a structural hypothesis requiring experimental confirmation.

In contrast, the three substitutions at Cys370 produced small-magnitude ΔΔG values in both predictors (DynaMut2: C370S = −0.93, C370Y = −0.64, and C370F = −0.52 kcal/mol; I-Mutant v2.0: −0.49, +0.44, and −0.67 kcal/mol, respectively). Although DynaMut2 labelled all three substitutions as “destabilising”, it should be noted that this tool classifies any ΔΔG below zero as destabilizing without applying a magnitude threshold; given its reported root-mean-square error of approximately 1.0–1.14 kcal/mol, predicted changes smaller than approximately 1 kcal/mol fall within the tool's error margin and cannot be interpreted as meaningful destabilization. For C370Y, the two tools disagreed in the predicted direction (I-Mutant v2.0 +0.44 versus DynaMut2 −0.64 kcal/mol), a discordance that reinforces the interpretation that this uncharacterized substitution exerts only a localized, low-confidence effect. The contrast between the large-magnitude predictions at position 352 and the small-magnitude predictions at position 370 was preserved consistently across both methodologically independent predictors. This pattern is consistent with the experimental observation that C370S enhances rather than impairs secretion (Arking et al., 2002) and indicates that position 370 is more tolerant of substitution than position 352. Together, these results support a residue-specific structural interpretation in which Phe352 appears more sensitive to disruptive substitution than Cys370. This pattern is consistent with the experimentally observed secretion-impairing effect of F352V and the

secretion-enhancing effect of C370S, while identifying C370Y, C370F, and F352I as variants that warrant further experimental characterization. Full results are presented in Table 2.

Table 2. In silico functional prediction and predicted thermodynamic perturbation for the five missense substitutions at positions 370 and 352 of the *KL* gene.

SNP ID	Substitution	PolyPhen Score	PolyPhen Prediction	PROVEAN Score	PROVEAN Prediction	PANTHER Prediction	PhD-SNP	SNPs&GO	I-Mutant v2.0 (ΔΔG)	DynaMut2 (ΔΔG)
rs9527025	C370Y	0.920	Possibly damaging	0.173	Neutral	Probably benign (Pdel = 0.02)	Disease	Disease (0.718)	Increase Stability (+0.44)	Destabilising (−0.64)
	C370S	0.014	Benign	4.026	Neutral	Probably benign (Pdel = 0.02)	Neutral	Neutral (0.354)	Decrease Stability (−0.49)	Destabilising (−0.93)
	C370F	0.791	Possibly damaging	−0.561	Neutral	Probably benign (Pdel = 0.02)	Disease	Disease (0.797)	Decrease Stability (−0.67)	Destabilising (−0.52)
rs9536314	F352V	1.000	Probably damaging	−6.994	Deleterious	-	Disease	Disease (0.528)	Decrease Stability (−3.02)	Destabilising (−1.52)
	F352I	1.000	Probably damaging	−5.995	Deleterious	-	Disease	Disease (0.414)	Decrease Stability (−1.56)	Destabilising (−1.25)

Note: ΔΔG values represent predicted thermodynamic perturbation estimates, not direct biophysical measurements. I-Mutant v2.0 (Capriotti et al., 2005) is a sequence/structure-based SVM applied to UniProt Q9UEF7. DynaMut2 (Rodrigues et al., 2021) combines normal-mode analysis with graph-based structural signatures, applied to the AlphaFold model of α-Klotho (AF-Q9UEF7-F1, chain A; pLDDT > 95 at both positions 352 and 370). DynaMut2 classifies any ΔΔG < 0 as destabilizing without a magnitude threshold; given its reported RMSE of approximately 1.0–1.14 kcal/mol, predicted changes smaller than ~1 kcal/mol fall within the tool's error margin and are interpreted as minimal perturbation. Negative ΔΔG = predicted destabilization; positive = predicted stabilization. PANTHER results were not available for rs9536314 substitutions. KL-VS = substitution present in the naturally occurring KL-VS haplotype.

3.3. Tissue-Specific Expression

GTEx v10 analysis of *KL* expression across 54 human tissues confirmed a strongly kidney-predominant pattern. Median expression was highest in kidney cortex (approximately 18.79 TPM), followed by kidney medulla (approximately 10.91 TPM). Moderate expression was detected in adipose subcutaneous (approximately 6.80 TPM), lung (approximately 6.35 TPM), and breast mammary tissue (approximately 4.89 TPM). Expression was near-absent in liver (approximately 0.07 TPM) and cultured fibroblasts (approximately 0.02 TPM), confirming that *KL* is not ubiquitously expressed.

This expression pattern is anatomically consistent with α-Klotho localization in renal distal tubule epithelial cells, where it serves as the membrane-bound FGF23 co-receptor regulating phosphate excretion and 1,25-dihydroxyvitamin D production (Hu et al., 2011; Kuro-o, 2019; Xu & Sun, 2015). The kidney also constitutes the primary source of circulating soluble Klotho, reinforcing its prominent role in the FGF23-Klotho endocrine axis. The functional implication is that any variant reducing Klotho expression or impairing its secretion from renal distal tubule cells would most directly affect the kidney-specific FGF23 signaling axis, with secondary consequences for circulating Klotho levels and systemic phosphate regulation. This tissue specificity means that the predicted structural perturbation of F352V is not equally relevant across all tissues but is functionally concentrated in the organ where *KL* expression and Klotho-dependent signaling are highest.

Integration of expression data with functional predictions contextualizes the potential impact of rs9536314 in tissue-specific terms. Experimental evidence that F352V impairs secretion from Klotho-expressing cells (Arking et al., 2002) suggests that such secretion impairment would be expected to

predominantly affect renal FGF23 co-receptor function and circulating Klotho levels, given the tissue-predominant expression pattern. The clinical association of rs9536314 with salt-sensitive hypertension in a large treatment-naive hypertensive cohort, manifested as a right-shifted pressure-natriuresis relationship, provides supporting evidence that this variant has functional relevance specifically within the kidney (Citterio et al., 2020). The near-absent expression in liver and fibroblasts suggests that molecular consequences of these variants are likely to be highly context-specific, with functional relevance most concentrated in the renal compartment. Moderate extra-renal expression in adipose and lung tissue suggests possible secondary roles in oxidative stress regulation and metabolic homeostasis (Xu & Sun, 2015). **Figure 2** presents the tissue expression violin plot for *KL* based on GTEx v10.

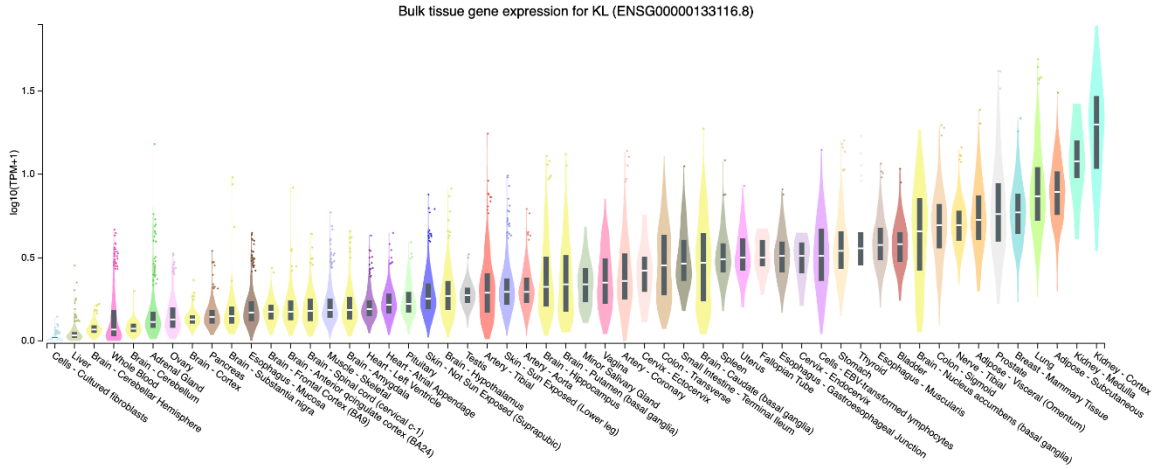

Figure 2. Violin plot of *KL* expression (log10 TPM+1) across human tissues based on GTEx v10 data.

3.4. Gene Interaction Network

The GeneMANIA network query for *KL* in Homo sapiens (default settings, all interaction categories enabled; web application v3.6.0; database August 13, 2021) retrieved a network of 21 nodes and 437 edges. The network comprised the FGF ligand family (FGF8, FGF9, FGF16, FGF17, FGF19, FGF20, FGF22, FGF23), the four FGF receptors (FGFR1–FGFR4), the paralog β-Klotho (KLB), lactase and lactase-like (LCT, LCTL), the calcium channel TRPV5, and four WNT ligands (WNT1, WNT3, WNT4, WNT5A). According to the GeneMANIA network weight, which the GeneMANIA documentation defines as the relevance of each data source for predicting the function of the query gene, edge contributions were dominated by physical interactions (77.64%), followed by co-expression (8.01%), predicted interactions (5.37%), co-localization (3.63%), genetic interactions (2.87%), shared pathway (1.88%), and shared protein domains (0.60%). For completeness and full reproducibility, the raw edge counts before GeneMANIA weighting were physical 216, shared protein domains 92, pathway 86, co-expression 19, predicted 12, genetic 7, and co-localization 5; the discrepancy between network weight and raw edge count reflects GeneMANIA's algorithmic re-weighting of each data source by its informativeness for the query gene.

KL was directly connected to all 20 other nodes in the network. Ranked by the number of supporting edges, the most densely connected neighbour of *KL* was FGF23 (5 edges; cumulative weight 2.05, including 4 physical-interaction edges and 1 pathway edge), followed by FGF19, FGFR1, FGFR2, FGFR3, FGFR4, and KLB (each with 4 edges). The remaining FGF ligands (FGF8, FGF9, FGF16, FGF17, FGF20, FGF22) were connected by 3 edges each, while WNT1, LCT, and LCTL were connected by 2 edges, and WNT3, WNT4, WNT5A, and TRPV5 by 1 edge each. The prominence of FGF23 as the most densely connected partner is concordant with the well-characterized direct molecular interaction between α-Klotho and FGF23 (Chen et al., 2018).

The FGF/FGFR cluster (shown in Figure 3) reflects the well-characterized ternary signaling complex through which α-Klotho mediates phosphate and vitamin D regulation (Hu et al., 2011; Kuro-o, 2019). Because the KL1 domain forms the structural interface that enhances FGF23 binding affinity to FGFRs, a predicted structural perturbation at Phe352 could influence the assembly of this ternary complex and modulate downstream MAPK/ERK activation. Combined with the kidney-predominant expression pattern from GTEx (Section 3.3), this network topology suggests that the primary

functional consequence of rs9536314 may concentrate at the renal FGF23–FGFR interface, potentially affecting phosphate excretion and vitamin D biosynthesis more prominently than other tissues where Klotho expression is lower. Additional connections to WNT pathway components (WNT1, WNT3, WNT4, WNT5A) support the reported function of α-Klotho as a modulator of Wnt/β-catenin signaling involved in cellular senescence, fibrosis, and carcinogenesis (Tang et al., 2016; Kuro-o, 2019; Ligumsky et al., 2022). Association with TRPV5 further reflects the role of Klotho in renal distal-tubule calcium-channel regulation (Wolf et al., 2014; Lee et al., 2021).

The network analysis above is descriptive in scope. Formal topological metrics such as betweenness, closeness, or eigenvector centrality are best computed on a curated organism-wide interactome rather than on a query-centric GeneMANIA network, because GeneMANIA expands outward from the query gene and therefore biases all centrality scores in favor of the query. We therefore deliberately refrain from formal centrality claims and identify topological analysis using a confidence-filtered STRING interactome, alongside pathway enrichment analysis (for example with Enrichr or g:Profiler), as priorities for follow-up work.

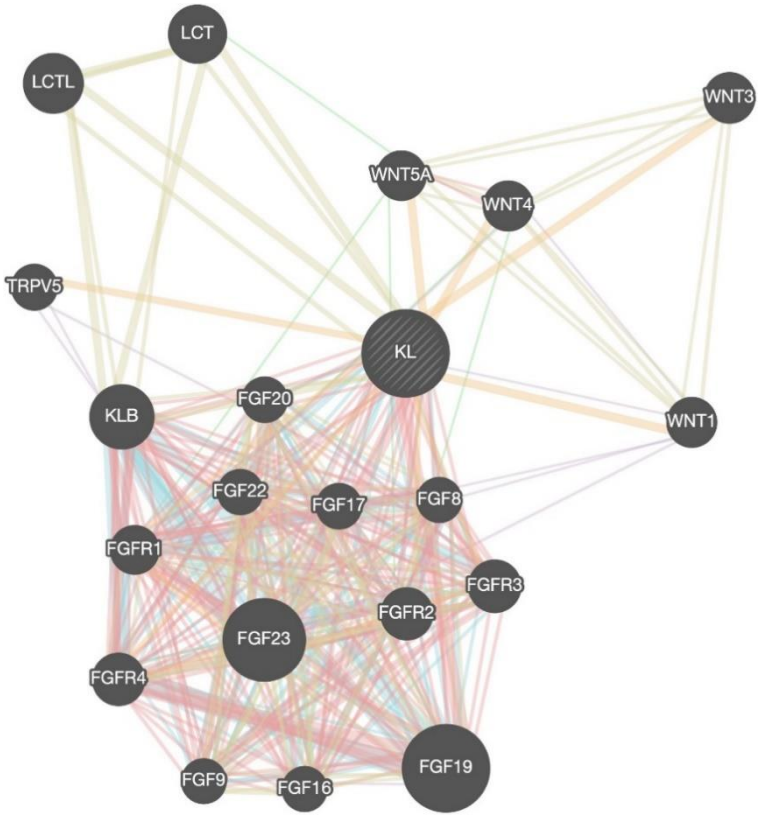

Figure 3. Gene interaction network of *KL* (Klotho) from GeneMANIA analysis. Edge colors indicate interaction types: pink = physical interactions; purple = co-expression; orange = predicted interactions; light blue = co-localization; green = genetic interactions; yellow/cream = shared pathways; gray = shared protein domains.

3.5. Integration with Experimental Evidence and Methodological Considerations

Several methodological considerations should be noted when interpreting these findings. Thermodynamic perturbation was estimated using two methodologically distinct predictors, I-Mutant v2.0 and DynaMut2, providing cross-tool comparison rather than reliance on a single algorithm. However, these tools estimate folding free-energy changes computationally and should not be considered equivalent to direct biophysical measurements such as differential scanning fluorimetry or circular dichroism. Additional evaluation using structure-based force-field approaches, such as FoldX or mCSM, would further strengthen the interpretation, particularly for the small-magnitude predictions at position 370. Although the AlphaFold model used in this study showed very high local confidence at both residues of interest, explicit conformational sampling was not performed. Future molecular dynamics simulation and protein–protein docking of KL1 variants within the FGF23–FGFR complex

would allow more direct assessment of conformational effects and co-receptor assembly. Similarly, the GeneMANIA network analysis was used descriptively, and formal topological metrics would be more appropriately computed using a curated organism-wide interactome. Because this study did not include new genotype data or clinical association testing, the clinical relevance of these variants was interpreted in relation to previously published studies.

Despite these methodological boundaries, the integrated evidence converges on a coherent residue-specific interpretation. F352V showed consistent deleterious predictions across multiple functional tools, relatively large negative ΔΔG values across two independent thermodynamic estimators, localization within a structurally constrained hydrophobic core, and biological relevance within the kidney-predominant FGF23–Klotho signaling context. Together, these findings provide a plausible structural explanation for the previously reported secretion-impairing phenotype of F352V. In contrast, the small-magnitude and partly discordant predictions for C370Y and C370F suggest localized effects of lower confidence and highlight these uncharacterized substitutions as candidates for experimental clarification. The absence of a significant association between rs9536314 or rs9527025 and all-cause or cardiovascular mortality in a prospective cohort of elderly Swedish men indicates that structural perturbation does not necessarily result in broad clinical outcomes, suggesting that KL-VS effects may be context-dependent. Rather than reassessing clinical association, this study provides a structural and mechanistic framework for prioritizing Klotho variants for protein-trafficking assays, three-dimensional structural studies, and population-specific genetic investigation.

4. Conclusion

This integrative in silico study provides structural and biological interpretations of the Klotho missense variants rs9527025 and rs9536314, with a focus on the contrasting secretion phenotypes of the KL-VS substitutions F352V and C370S. Multi-algorithm functional prediction together with thermodynamic perturbation analysis indicated that substitutions at Phe352, particularly F352V, produce the most consistent predicted structural disruption within the KL1 hydrophobic core. This pattern is consistent with the experimentally reported secretion-impairing effect of F352V. C370S, in contrast, showed only small-magnitude predicted perturbation within the expected error range of the stability predictors, in line with its reported secretion-enhancing phenotype. The uncharacterized C370Y and C370F substitutions produced lower-confidence and partly discordant predictions, suggesting localized effects that require experimental clarification. Integration with GTEx v10 expression data and GeneMANIA network analysis further situates these variants within the kidney-predominant FGF23 - Klotho endocrine axis, particularly in relation to renal mineral metabolism and circulating Klotho biology. Taken together, these findings prioritize Phe352 as a structurally sensitive residue and suggest future validation through protein-trafficking assays, biophysical stability measurements, molecular dynamics simulation, and population-specific association studies. More broadly, this analysis shows how computational prediction can be anchored to existing experimental evidence to guide mechanistic interpretation of missense variants.

REFERENCES

Arking, D. E., Krebsova, A., Macek, M., Sr., Macek, M., Jr., Arking, A., Mian, I. S., Fried, L., Hamosh, A., Dey, S., McIntosh, I., & Dietz, H. C. (2002). Association of human aging with a functional variant of klotho. *Proceedings of the National Academy of Sciences of the United States of America*, 99(2), 856-861. https://doi.org/10.1073/pnas.022484299

Betz, S. F. (1993). Disulfide bonds and the stability of globular proteins. *Protein Science*, 2(10), 1551-1558. https://doi.org/10.1002/pro.5560021002

Dalton, G. D., Xie, J., An, S. W., & Huang, C. L. (2017). New insights into the mechanism of action of soluble klotho. *Frontiers in Endocrinology*, 8, 323. https://doi.org/10.3389/fendo.2017.00323

Capriotti, E., Fariselli, P., & Casadio, R. (2005). I-Mutant2.0: predicting stability changes upon mutation from the protein sequence or structure. Nucleic Acids Research, 33(suppl_2), W306–W310. https://doi.org/10.1093/nar/gki375

Citterio, L., Delli Carpini, S., Lupoli, S., Brioni, E., Simonini, M., Fontana, S., Zagato, L., Messaggio, E., Barlassina, C., Cusi, D., Manunta, P., & Lanzani, C. (2020). Klotho gene in human salt-sensitive hypertension. Clinical Journal of the American Society of Nephrology, 15(3), 375-383. https://doi.org/10.2215/CJN.08620719

Chen, G., Liu, Y., Goetz, R., Fu, L., Jayaraman, S., Hu, M. C., Moe, O. W., Liang, G., Li, X., & Mohammadi, M. (2018). α-Klotho is a non-enzymatic molecular scaffold for FGF23 hormone signalling. Nature, 553(7689), 461–466. https://doi.org/10.1038/nature25451

Doi, S., Zou, Y., Togao, O., Pastor, J. V., John, G. B., Wang, L., Shiizaki, K., Gotschall, R., Schiavi, S., Yorioka, N., Takahashi, M., Boothman, D. A., & Kuro-o, M. (2011). Klotho inhibits transforming growth factor-beta1 (TGF-beta1) signaling and suppresses renal fibrosis and cancer metastasis in mice. Journal of Biological Chemistry, 286(10), 8655-8665. https://doi.org/10.1074/jbc.M110.174037

Hu, M. C., Shi, M., Zhang, J., Quinones, H., Griffith, C., Kuro-o, M., & Moe, O. W. (2011). Klotho deficiency causes vascular calcification in chronic kidney disease. Journal of the American Society of Nephrology, 22(1), 124-136. https://doi.org/10.1681/ASN.2009121311

Kanbay, M., Copur, S., Ozbek, L., Mutlu, A., Cejka, D., Ciceri, P., Cozzolino, M., & Haarhaus, M. L. (2023). Klotho: a potential therapeutic target in aging and neurodegeneration beyond chronic kidney disease-a comprehensive review from the ERA CKD-MBD working group. Clinical kidney journal, 17(1), sfad276. https://doi.org/10.1093/ckj/sfad276

Kuro-o, M. (2019). The Klotho proteins in health and disease. Nature Reviews Nephrology, 15, 27-44. https://doi.org/10.1038/s41581-018-0078-3

Kuro-o, M., Matsumura, Y., Aizawa, H., Kawaguchi, H., Suga, T., Utsugi, T., Ohyama, Y., Kurabayashi, M., Kaname, T., Kume, E., Iwasaki, H., Iida, A., Shiraki-Iida, T., Nishikawa, S., Nagai, R., & Nabeshima, Y. (1997). Mutation of the mouse klotho gene leads to a syndrome resembling ageing. Nature, 390, 45-51. https://doi.org/10.1038/36285

Neitzel, J., Franzmeier, N., Rubinski, A., Dichgans, M., Brendel, M., Alzheimer's Disease Neuroimaging Initiative (ADNI), Malik, R., & Ewers, M. (2021). KL-VS heterozygosity is associated with lower amyloid-dependent tau accumulation and memory impairment in Alzheimer's disease. Nature communications, 12(1), 3825. https://doi.org/10.1038/s41467-021-23755-z

Rodrigues, C. H. M., Pires, D. E. V., & Ascher, D. B. (2021). DynaMut2: Assessing changes in stability and flexibility upon single and multiple point missense mutations. Protein Science, 30(1), 60–69. https://doi.org/10.1002/pro.3942

Tang, X., Wang, Y., Fan, Z., Ji, G., Wang, M., Lin, J., Huang, S., & Meltzer, S. J. (2016). Klotho: A tumor suppressor and modulator of the Wnt/beta-catenin pathway in human hepatocellular carcinoma. Laboratory Investigation, 96(2), 197-205. https://doi.org/10.1038/labinvest.2015.86

Tokuriki, N., & Tawfik, D. S. (2009). Stability effects of mutations and protein evolvability. Current Opinion in Structural Biology, 19, 596-604. https://doi.org/10.1016/j.sbi.2009.08.003

Wolf, M. T., An, S. W., Nie, M., Bal, M. S., & Huang, C. L. (2014). Klotho up-regulates renal calcium channel transient receptor potential vanilloid 5 (TRPV5) by intra- and extracellular N-glycosylation-dependent mechanisms. Journal of Biological Chemistry, 289(52), 35849-35857. https://doi.org/10.1074/jbc.M114.616649

Wu, P. H., Westerberg, P. A., Kindmark, A., Tivesten, A., Karlsson, M. K., Mellstrom, D., Ohlsson, C., Fellstrom, B., Linde, T., & Ljunggren, O. (2020). The association between single nucleotide polymorphisms of Klotho gene and mortality in elderly men: The MrOS Sweden study. Scientific Reports, 10, 10243. https://doi.org/10.1038/s41598-020-66517-5

Ligumsky, H., Merenbakh-Lamin, K., Keren-Khadmy, N., Wolf, I., & Rubinek, T. (2022). The role of α-klotho in human cancer: molecular and clinical aspects. Oncogene, 41(40), 4487–4497. https://doi.org/10.1038/s41388-022-02440-5

Xu, Y., & Sun, Z. (2015). Molecular basis of Klotho: From gene to function in aging. Endocrine Reviews, 36(2), 174-193. https://doi.org/10.1210/er.2013-1079

Zhu, Z., Xia, W., Cui, Y., Zhen, J., Hao, Y., Yin, S., Wang, D., Meng, S., & Han, S. (2019). Klotho gene polymorphisms are associated with healthy aging and longevity: Evidence from a meta-analysis. Mechanisms of Ageing and Development, 178, 33-40. https://doi.org/10.1016/j.mad.2018.12.003